DYNAMIC ROTORCRAFT APPLICATIONS USING OVERSET GRIDS

Mark Potsdam
Aeroflightdynamics Directorate (AMRDEC)
U.S. Army Research, Development, and Engineering Command
Moffett Field, CA, USA

ABSTRACT

Computational fluid dynamics (CFD) for rotorcraft applications has made significant gains in the past years. One of the enabling technologies has been the use of structured overset grids and flow solvers, which ease the grid generation burden for complex helicopter configurations compared with other structured grid methods. They allow for moving body components in relative motion that are typical of rotorcraft configurations. Overset CFD software has been used for isolated rotors in hover and forward flight as well as complex rotor-fuselage interaction problems. This work describes some of the advanced calculations that have been performed using overset grids and high performance computing at the U.S. Army Aeroflightdynamics Directorate.

NOTATION

C_Q	rotor torque coefficient
C_T	rotor thrust coefficient
FM	rotor figure of merit, $C_T\sqrt{C_T/2}/C_Q$
M	Mach number
M^2c_m	section pitching moment
M^2c_n	section normal force
PUWSS	pitch-up with sideslip
r	radial coordinate
R	blade radius
TPP tilt	equivalent tip path plane tilt
σ	rotor solidity
Ψ	rotor azimuth, degrees (0 deg aft)

INTRODUCTION

Analysis of helicopter fuselages and rotors is an exceptionally challenging multidisciplinary problem. Successful aerodynamic analysis of this problem requires accurate capabilities for modeling unsteady, three-dimensional flowfields, including incompressible flow, transonic flow with shocks, reversed flow, dynamic stall, vortical wakes, rigid body motion, and aeroelastic deformation. To handle the overwhelming complexity of the problem, rotorcraft comprehensive codes, which attempt to cover most of the multidisciplinary aspects (aerodynamics, structures, dynamics, acoustics, stability and control, and propulsion), use lower-order aerodynamics models based on lifting line theory.

In the meantime, computational fluid dynamics (CFD) for rotorcraft applications has made significant gains in the past years, however, still lagging far behind their fixed wing counterparts due to geometry and flowfield complexity. One of the enabling technologies has been the use of overset grids and flow solvers, which ease the grid generation burden for complex helicopter configurations compared with other structured grid methods, while allowing for moving body components in relative motion that are typical of rotorcraft configurations. Overset CFD software has been used for viscous, dynamic simulations of isolated rotors in hover and forward flight as well as complex rotor-fuselage interaction problems. The National Rotorcraft Technology Center Rotorcraft Centers of Excellence in the U.S. have made progress in dynamic rotorcraft simulations at the University of Maryland [1] and Georgia Institute of Technology [2,3,4]. The recently completed French-German CHANCE project and other researchers in Europe have demonstrated dynamic, moving body capabilities [5,6,7,8]. Unstructured, moving body grids with mesh adaption have been investigated in Korea [9].

The overset grid domain decomposition methodology was originally proposed by Steger [10]. In the "Chimera" method, the grid generation task about a geometrically complex configuration is reduced to multiple, overlapping grids covering the domain. The result is multiple, simple topology meshes communicating through boundary interpolation. Wall-bounded viscous layer resolution, moving bodies, and parallel processing methods are especially easy to accommodate. Implementation in either structured or unstructured grid CFD codes is straightforward with the use of an IBLANK array. The penalty for simplification of the grid generation task is the burden to provide boundary interpolation data and hole cutting. Hole cutting is required when grid points fall inside inappropriate regions, such as inside solid bodies. A wide range of CFD codes take advantage of this technique through library support [11,12] or independent development efforts. Several overset codes are now being used for rotorcraft calculations. For example, all three codes in Ref. 2 have overset capability under development.

Presented at the 31st European Rotorcraft Forum, September 13-15, 2005, Florence, Italy.

Lumping all rotorcraft applications together is a mistake. In particular, tiltrotor and helicopter rotors have significant differences in design philosophy and geometric representation. Small-scale, low Reynolds number rotorcraft and UAVs, ducted fans, and new, advanced configurations, such as the Canard Rotor Wing, present special challenges for CFD modeling. The ability to accurately analyze and understand diverse flow regimes is a critical requirement for optimum rotorcraft design.

Significant advances have been made in modeling complex, moving body configurations in time-dependent simulations by taking advantage of the overset grid method and continual advances in high performance computing. However, several roadblocks remain. In particular, current applications indicate the inability to accurately model the rotorcraft wake due to excessive numerical dissipation and lack of grid resolution. Turbulence modeling also continues to prevent revolutionary progress in dynamic stall predictions. This paper discusses recent progress at the U.S. Army Aeroflightdynamics Directorate (AFDD) in using overset grid methods and high performance computing for rotorcraft performance prediction and flowfield simulations. The computational methodology is described, followed by example calculations for hover, forward flight, and rotor-fuselage interaction.

METHODOLOGY

Numerous tools have been developed to simplify and expedite the process for overset solution methodologies. While these tools help tremendously, the overset grid CFD process is far from automated. Many researchers from NASA, U.S. Army, government contractors, and industry have contributed to the software development.

Overset structured grid generation is performed using the powerful graphical user interface OVERGRID [13,14], developed by William Chan at NASA Ames. The software contains capability for geometry and grid visualization, processing, and diagnosis; surface and volume grid generation; flow solver input preparation; dynamic motion simulation; and hole-cutting pre-processing. The program is written in C, OpenGL, Tcl/Tk, and FORTRAN and has been ported to most UNIX and LINUX platforms. Surface grid generation can be performed on structured or unstructured surface entities. The overset surface grid generation process typically involves a hyperbolic marching scheme for surface generation (SURGRD), starting from an intersection, feature, or arbitrary curve. Transfinite interpolation can be used for domains bounded on more than one side. Hyperbolic grid generation (HYPGEN) is effectively used for volume grid generation of body-conforming meshes. End spacings are specified in the 2D and 3D grid generation process, and limitations on stretching ratio can be maintained.

Flow solutions are computed on structured, overset grids using body-conforming, curvilinear “near-body” grids and automatically generated uniform Cartesian “off-body” grids as developed by Meakin [15]. Near-body grids, generated in OVERGRID, are used to discretize the surface geometries and capture wall-bounded viscous effects. They typically extend about one (characteristic) chord length from the surface. Multi-level, uniform Cartesian off-body grids extend to the farfield with increasing grid spacing (factor of 2) and capture the off-body flow field including wakes. An example of this gridding strategy is shown in Figure 15. Level-1 grids, shown in red, have the finest uniform spacing.

Force and moment evaluation is performed using the FOMOCO software [16,17]. With arbitrary, multiply defined surfaces in the overset methodology, integration of aerodynamic quantities is a difficult problem. In the MIXSUR module of FOMOCO, singly defined regions of the surface geometry are created using overset blanking methodology. These regions are then connected by unstructured, triangular “zipper” grids. The OVERINT integration routine uses the structured and unstructured regions to perform pressure, momentum, and viscous force and moment integrations. This module is integrated directly into the flow solver.

The flow solver used by the U.S. Army AFDD rotorcraft group is the Reynolds-averaged Navier-Stokes computational fluid dynamics code OVERFLOW 2 [18]. It is continually being developed by NASA and the U.S. Army and has been applied to a wide range of fluid dynamics problems. OVERFLOW 2 is the result of the recent merging of the capabilities of OVERFLOW-D [19] and OVERFLOW 1.8 [20,21] by Pieter Buning at NASA Langley. OVERFLOW-D is now replaced by OVERFLOW 2, which has acquired most of the OVERFLOW-D capabilities. These capabilities include 6-degree-of-freedom, dynamic, rigid-body motion; automatic, background Cartesian grid generation; hole cutting and domain connectivity; solution adaption; and MPI parallel processing. The latest OVERFLOW 1.8 upgrades include steady and unsteady low Mach number preconditioning, advanced 1- and 2-equation turbulence models, dual time stepping, multigrid acceleration, matrix dissipation, and upwind schemes. OVERFLOW 2 thus contains numerous algorithm and turbulence model options for a parallel processing environment.

Most of the calculations shown here use OVERFLOW-D, which is based on an earlier version of OVERFLOW. For spatial discretization, 4^{th}-order central differencing with artificial dissipation is used. For subsonic rotorcraft flows the 2^{nd}-order artificial dissipation is typically turned off. When possible, grids overlap sufficiently to allow double fringing, where two boundary points are interpolated from adjacent overlapping grids.

This allows gradient as well as solution information to be transferred more smoothly and accurately between grids. The time-accurate analyses use an implicit 1st-order algorithm in the near-body grids and an explicit 3rd-order Runge-Kutta scheme in the off-body grids. The Baldwin-Barth one-equation turbulence model is used in the near-body grids, which are assumed fully turbulent. Thin-layer viscous terms are added only in the computational direction normal to the surface. Off-body grids are modeled as inviscid in order to reduce the numerical dissipation in the wake. More recent investigations with OVERFLOW 2 [2] are using advanced turbulence models, low Mach number preconditioning, and 2nd-order dual time stepping.

For rotorcraft problems, modifications to the code were made for calculation of isolated hovering rotors by Strawn [22]. In particular, isolated, hovering rotor flows can be computed as steady-state problems in a blade-fixed reference frame with the addition of a rotational source term. Special hover characteristic outer boundary conditions based on a source-sink distribution have also been used. An LU-SGS time advancement algorithm is combined with local time stepping to speed convergence to steady state. Symmetry considerations in multi-bladed rotors can be used to significant advantage to reduce problem size. OVERFLOW 2 also contains momentum source, blade element actuator disk capability that can be used as a modeling simplification to individual blade modeling [23].

More complex configurations with bodies in relative motion require the time-accurate modeling of the moving bodies. XML inputs or user-defined FORTRAN subroutines prescribe the arbitrary six degree-of-freedom motions. XML motion input is conveniently linked with the OVERGRID GUI [24] and allows for hierarchical motions of aerodynamic components. In addition to prescribed motion, aerodynamic forces can also be applied.

Motion of overset grids requires recalculation of the domain connectivity, including hole cuts and intergrid boundary point interpolation coefficients, at each time step, as the near-body grids move through the stationary off-body grids. Hole cutting, which is required when one grid passes through another, is performed efficiently using Meakin's object X-ray technique [25]. For rigid bodies, X-rays are generated in a pre-processing step using OVERGRID. Interpolation coefficients are determined using inverse maps, stencil walks, and Newton iteration searching. For moving body problems, reuse of information from the previous time step enables an order of magnitude speed-up compared to domain connectivity solutions from scratch. Using this technique, the domain connectivity work can be efficiently performed in less than 10-20% of the time required for the flow solver.

For aeroelastic calculations, several modifications are made to the rigid body version of OVERFLOW-D [26]. Capability that has been added to accurately account for deforming surface grids includes implementation of the Geometric Conservation Law and finite volume time metrics, surface grid deformation and volume grid movement, and subroutine-activated regeneration of X-rays and inverse maps. Particularly for rotor blades, elastic motion is introduced by the structural mechanics and dynamics in addition to rigid body movement due to rotor rotation, collective, and cyclic. Surface point motion is computed from a transformation matrix that contains both the translational and rotational motions determined from quarter chord motion. Volume grid points are moved using the motion of the associated constant computational coordinate surface point. Outer boundaries are free to float, allowing for unlimited flapping of rotor blades without constraints on grid generation.

High aspect ratio edgewise helicopter rotors in hover and forward flight have significant rotor dynamics and aeroelastics which usually cannot be neglected, hence the need for CFD and computational structural dynamics (CSD) coupling. An efficient loose coupling algorithm is implemented which gives fast convergence to a periodic, trimmed state. In an iterative fashion the methodology completely replaces the comprehensive code airloads with CFD airloads, while in the process using lifting line aerodynamics to trim and CSD to account for blade deformation. Both CAMRAD II and RCAS comprehensive codes are coupled [26].

Post-processing of large, time-dependent datasets can be very labor intensive, in addition to the computational expense of frequently saving the flow solution. Some flow visualization post-processing has been incorporated directly in OVERFLOW 2 by Tor Nygaard at Eloret Inc. Capability includes dumping of surface flowfield data and particle tracing. Co-processing particle tracing within OVERFLOW 2 using the parallel processing framework is more robust, accurate, efficient, and significantly less labor intensive than post-processing strategies. The major drawback is the requirement to know in advance the areas of interest in which to seed the flow or the solution must be rerun. However, due to the overwhelming file management issues required for post-processing large-scale, dynamic, time-accurate rotorcraft simulations, co-processing is an attractive alternative.

Solutions are computed on large parallel computers or a network of PCs/workstations communicating with the Message Passing Interface (MPI) protocol. Both the domain connectivity and flow solver modules have been parallelized for efficient, scalable computations using MPI [27,28]. Coarse grain parallelization on large numbers of processors is achieved by distributing grids among the processors, and if necessary, splitting them as appropriate into smaller blocks to prevent bottlenecks.

APPLICATIONS

Applications of the overset grid software for rotorcraft configurations are presented here for hover and forward flight of isolated rotors and rotor-fuselage combinations. The configurations under investigation are the UH-60A Blackhawk helicopter and the V-22 Osprey tiltrotor.

The UH-60A Blackhawk is a utility tactical transport helicopter with a contemporary, high performance, 4-bladed rotor. The blade has a radius of 322 inches, a reference (SC1095 airfoil) chord of 20.76 inches, and a 20 degree swept tip outboard of 93% span. The solidity is .0826, and there is approximately 16 degrees of nonlinear twist.

The V-22 is the first production tiltrotor and serves in transport and special operations roles. The 3-bladed rotors have a 228 inch radius, a tip chord of 22.0 inches, solidity of 0.105, and 38 degrees of nonlinear twist. The large amount of nonlinear twist is typical of tiltrotors but significantly different from helicopter configurations. Bell proprietary XN-series airfoils are used.

Isolated Hover

Although not actually a dynamic, moving body problem when simulations are performed in the reference frame of the hovering isolated rotor, hover is an exceptionally important part of rotorcraft operation. More than anything else, hover defines the unique capabilities of helicopters and tiltrotors. Accurately determining hover performance is critical in rotorcraft design. Numerous rotor configurations in hover have been investigated by U.S. Army personnel and collaborators using overset grid methods, including quarter-scale V-22 and JVX [29], UH-60A [22], Comanche FANTAIL™ [23,30], Mesicopter [31], and Mars rotor [32]. The scaled V-22 and UH-60A are highlighted here.

Model-Scale UH-60A [22]

A 17.5%-scale isolated rotor UH-60A model was tested in hover by Lorber [33]. The experimental dataset contains performance information as well blade sectional loadings. The hover tip Mach number is approximately 0.64.

Strawn and Djomehri performed several CFD calculations on the model-scale UH-60A in hover [22]. Measured blade elastic twist is used to define the aeroelastically deformed surface grid at each thrust condition. The UH-60A near-body grids for hover extend approximately 0.60 chords away from the body and include sufficient resolution to capture boundary layer viscous effects and y^+ at the wall less than one. The near-body grid system is shown in Figure 1. The grids use C-mesh topology blades and tip caps. Each blade contains 1.7 million points in 3 grids — blade, root cap, and tip cap. A centerbody grid is included to prevent flow recirculation at the axis. Only one blade is modeled in a quarter domain simulation with periodicity enforced at the appropriate boundaries. The total grid system contains 10.6 million points: 2.1 million near-body and 8.5 million off-body. Wake spacing on the finest Cartesian level is 0.10 times the reference chord. A total of five progressively coarser levels are generated out to the farfield boundary, which is placed at six rotor radii in all directions from the center of the domain.

CFD simulations were run for eight collective angles [22]. A comparison of figure of merit predictions against experimental test data, as shown in Figure 2, is excellent. Discrepancies are only noted at the lowest thrust level for which the CFD results showed poor convergence due to the close proximity of the rotor wake.

Quarter-Scale V-22 [29]

The Tilt Rotor Aeroacoustics Model (TRAM) is a quarter-scale V-22 wind tunnel model that was constructed to facilitate tiltrotor aeromechanics research. The isolated scaled V-22 rotor was tested in the Duits-Nederlandse Windtunnel Large Low-speed Facility (DNW-LLF) [34]. The test provided a significant source of aeroacoustics, performance, and structural loads data for validation of tiltrotor analyses. Among the aerodynamics data acquired were rotor performance and blade pressures. The nominal hover tip Mach numbers investigated in this test are 0.58 and 0.62, although this is not representative of the V-22.

Overset grids for the quarter-scale V-22 are similar in construction to the UH-60A configuration. However, elastic blade effects are minor in hover for these stiff blades and have not been included. The near-body grids extend approximately one tip chord away from the body. Each blade grid contains 1.9 million points. The total 3-bladed grid system with no periodicity assumed contains 15.9 million points: 6.2 million near-body and 9.7 million off-body. Wake spacing on the finest Cartesian level is 0.10 times the tip chord. The level-1 grid extends 0.6 rotor radii below the plane of the rotor. Where the Cartesian grid points fall inside the geometry, hole cutting is employed to blank out these points. A slice through the grid system in Figure 3 shows the off-body grids and hole cuts.

CFD solutions for the scaled V-22 rotor were run for a range of collective angles from 8 to 16 degrees with a tip Mach number of 0.625 [29]. Comparison of computations with the DNW hover performance data is shown in Figure 4, detailing figure of merit trends with thrust. The agreement for rotor performance is quite good. There is a consistent underprediction of figure of merit (0.01-0.02), with the correct trends predicted across the collective range. This discrepancy can be attributed to the fully turbulent assumption, when in actuality at these local chord Reynolds numbers, some laminar flow undoubtedly exists. This is supported by calculations with transition specified.

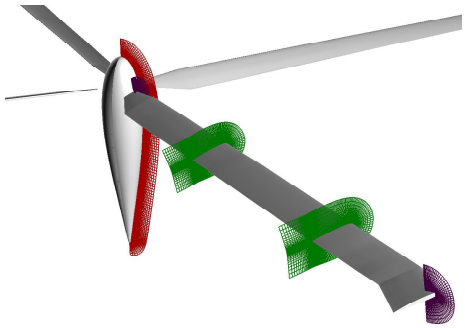

Figure 1. 17.5%-scale UH-60A near-body grid system in hover.

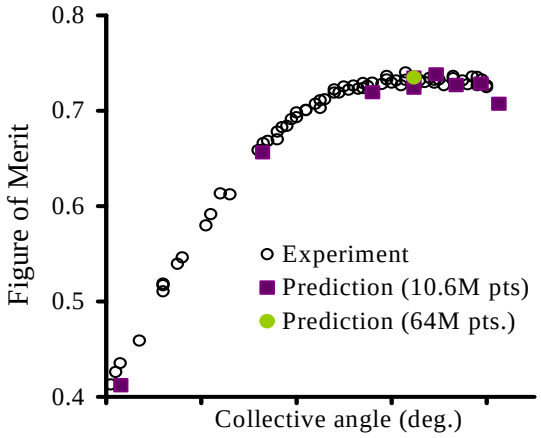

Figure 2. 17.5%-scale UH-60A figure of merit vs. collective.

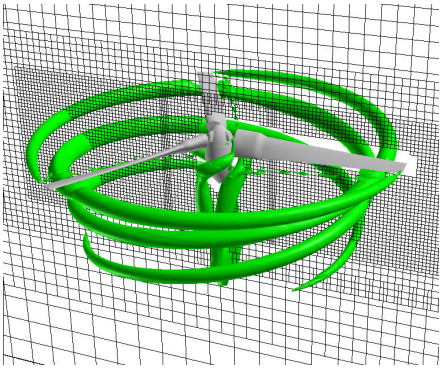

Figure 3. 0.25-scale V-22 off-body grid system and wake vorticity in hover.

Wake Resolution

Both configurations showed grid independence of the integrated hover performance quantities when off-body grid spacing was reduced from 0.10 chords to 0.05 chords, and, in the tiltrotor case, the surface grids were also refined (Figures 2 and 4). However, 64 million points for the UH-60A and 37.4 million points for the V-22 were still not enough to show grid convergence in the wake flowfield. Figure 5 shows wake vorticity contours for the baseline and fine grid V-22 rotor. Figure 6 shows spanwise thrust loading

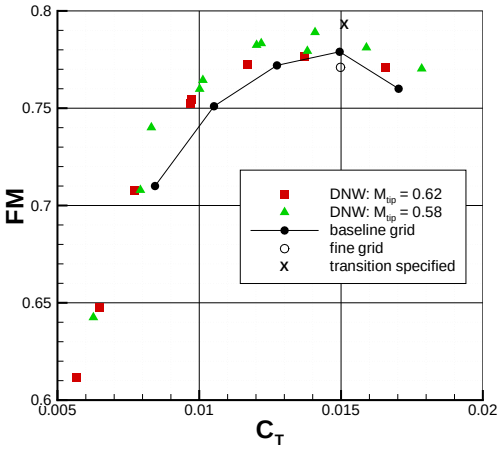

Figure 4. 0.25-scale V-22 figure of merit vs. thrust.

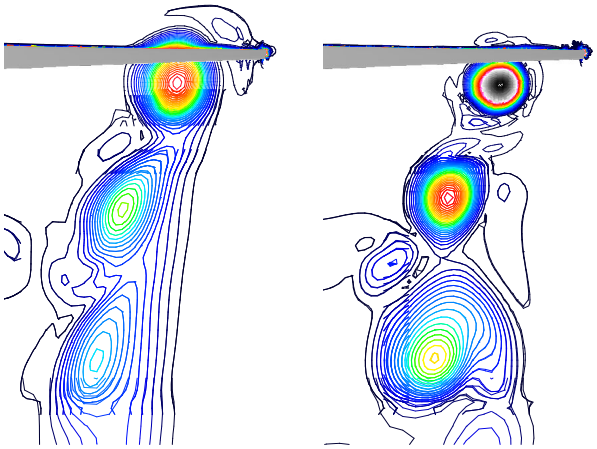

0.10 chords **0.05 chords**

Figure 5. 0.25-scale V-22 rotor wake vorticity at blade with varying wake spacing.

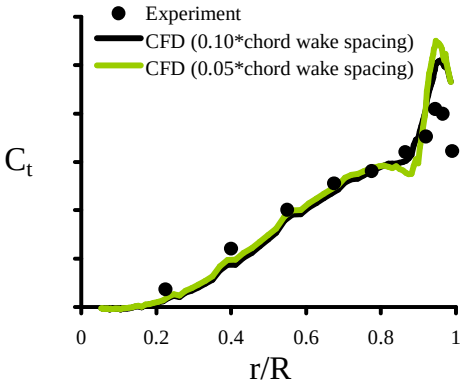

Figure 6. 17.5%-scale UH-60A sectional thrust with varying wake spacing.

(sectional C_t) for the baseline and fine grid UH-60A calculations. As indicated directly by the vortex wake structure and indirectly by the effect that core size and miss distance have on blade loadings, neither case can be considered grid converged for flowfield details.

This is not totally unexpected since the tip vortex core size is on the order of 0.10 chords, and is, therefore, in no sense resolved. Instead, the tip vortex is overly dissipated in all these calculations. It is estimated that a mere 10 points across the vortex core in a uniform Cartesian mesh will require billions of grid points. While such large grid systems are feasible on modern supercomputers with thousands of processors, the post-processing of such solutions becomes exceedingly cumbersome with current visualization methods. Adaptive mesh refinement methods may hold some promise for more judicious use of grid points for resolution of wake vortices.

The overall conclusions to be drawn from numerous discrete blade hover investigations of isolated rotors is that performance is generally well predicted by the overset grid CFD, however, the details of the flow, and the wake in particular, have not yet been shown to be fully resolved or grid converged. Accurate calculation of vortical wakes is one of the major deficiencies in rotorcraft CFD analyses.

Forward Flight

Calculations of edgewise rotorcraft in forward flight generally requires unsteady, dynamic simulations when discrete blade models are used. However, the V-22 rotor in forward flight is an axial propeller. Calculations have recently been performed for both the V-22 [35] and UH-60A [26] isolated rotors in level cruise flight.

Full-Scale UH-60A [26]

The UH-60A isolated rotor in forward flight has been extensively investigated by numerous researchers working with the NRTC/RITA UH-60 Airloads Workshop in order to understand key unsolved problems in rotor airloads prediction. A unique and extensive flight test database exists for this helicopter in level flight and transient maneuvers [36]. The data were obtained during the NASA/Army UH-60A Airloads Program. The database provides aerodynamic pressures, structural loads, control positions, and rotor forces and moments, allowing for the validation of both aerodynamic and structural models. The test matrix contains a wide range of advance ratios and gross weight coefficients. Note that since publication of Ref. 26 and in all publications after 2004, a 14-degree phase correction to the flight test data has been made [37].

The UH-60A rotor geometry as described above is used. The grid, however, is a high fidelity definition of the theoretical flight rotor blade including trim tab. The surface grids of the 4-bladed configuration are shown in Figure 7 along with the fuselage grid. Baseline off-body grid spacing is the typical 0.10 chords. The level-1 grid is specified a priori to contain the complete rotor wake in the vicinity of the rotor. In particular, it extends 0.3 rotor radii below the

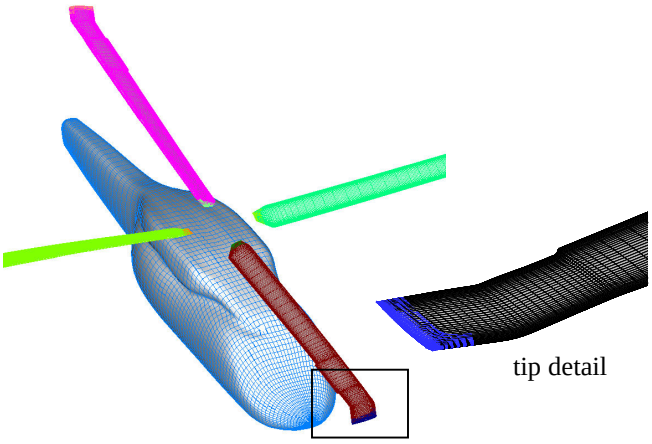

Figure 7. UH-60A forward flight surface grids.

plane of the rotor. Solution adaption is not used for rotorcraft problems because it is more expedient and efficient to pre-specify the complete wake region than to perform frequent and costly solution adaptions, which would most likely cover most of the wake anyway. The resulting grid system contains 26.1 million points: 14.4 million near-body and 11.7 million off-body. An azimuthal step size of 0.05 degrees is used in the CFD calculations, corresponding to 1800 iterations per 90 degrees of rotation of the 4-bladed rotor. The CFD/CSD coupled solutions use CAMRAD II and converge after 6-10 coupling iterations, with the coupling occurring every 90 degrees of rotor rotation. Periodic solutions are obtained by trimming to measured thrust and hub moment values.

Several level flight UH-60A data points have been used to test the accuracy, efficiency, and robustness of the CFD/comprehensive coupling procedure [26]. Flight counter c8534 is a high speed (158 knots), high advance ratio (0.37), level flight data point with $C_T/\sigma = 0.084$. Comparisons of the coupled OVERFLOW/CAMRAD results with flight test data and CAMRAD II free wake analysis are shown in Figure 8 for an outboard span station. The magnitudes of the normal force and especially the pitching moment from the coupled solution are in good agreement with the flight test data. The mean has been removed from the pitching moments due to possible flight test errors. The shape of the computed airloads curves are very good. Some discrepancies can be noted at this station, such as the shape of the minimum peak and a minor phase error, although these are improved at other radial locations High frequency oscillations in the test data in the first quadrant resulting from wake interaction are beginning to be captured. The phase and magnitude of the coupled airloads are a significant improvement over the free wake analysis.

A second flight test counter c8513 is a low speed (65 knots), low advance ratio (0.15), level flight data point with $C_T/\sigma = 0.076$. At this condition there are significant low

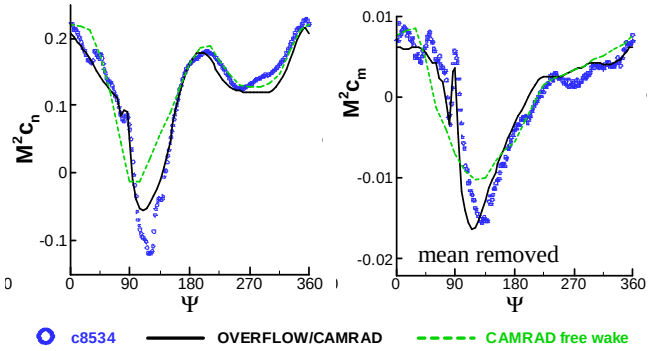

Figure 8. UH-60A airloads comparison, 0.37 advance ratio, r/R = 0.865.

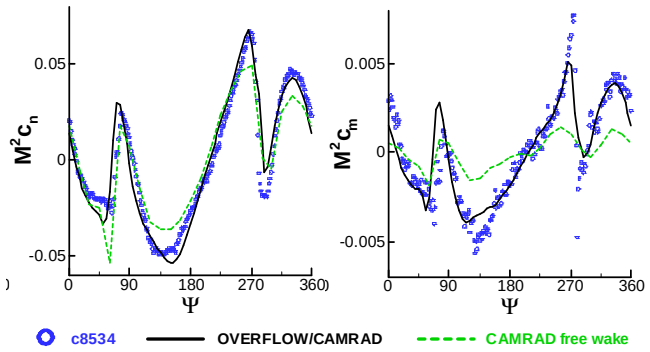

Figure 9. UH-60A airloads comparison (means removed), 0.15 advance ratio, r/R = 0.965.

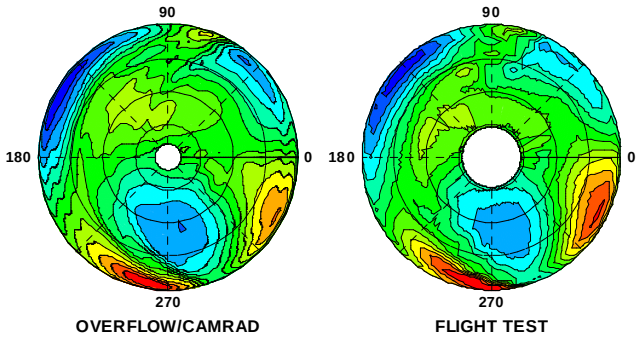

Figure 10. UH-60A rotor disk normal force comparison (mean removed), 0.15 advance ratio.

frequency blade-wake interactions which dominate the airloads. Comparisons of the coupled results with flight test data and CAMRAD II free wake analysis are shown in Figure 9 for an outboard span station. The phase and magnitudes of the normal force and pitching moment from the coupled solution are in excellent agreement with the flight test data. The blade-vortex interaction normal force impulses at 90 and 270 degrees azimuth are captured accurately and sharply. A qualitative comparison of normal force on the rotor disk is also in excellent agreement in Figure 10. The blade-vortex interactions are clearly visible. Visualization of the wake (Q criteria) in Figure 11 also

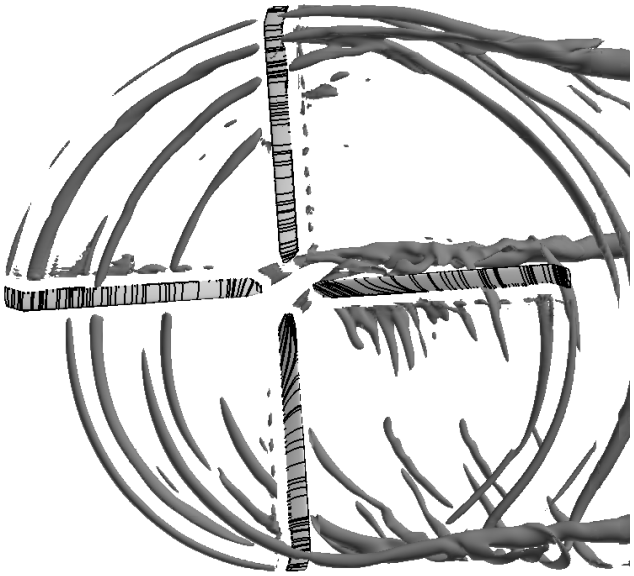

Figure 11. Wake visualization and surface streamlines, 0.15 advance ratio.

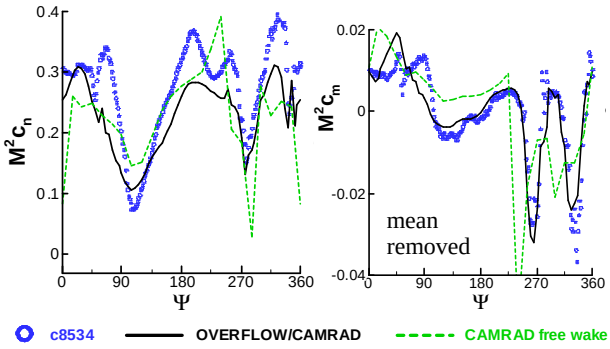

Figure 12. UH-60A airloads comparison, high C_T, 0.24 advance ratio, , r/R = 0.865.

shows the multiple blade-wake interactions. Several tip vortices from the blades are visible, but generally more than one revolution cannot be maintained in the off-body grids due to numerical dissipation in the wake.

A final flight counter c9017 is an intermediate speed (101 knots) and advance ratio (0.24), high thrust coefficient (C_T/σ = 0.129), level flight test point flown at 17,000 ft. This is a challenging and quintessential rotorcraft test case due to the wide variation of unsteady flow conditions, ranging from transonic to stall, with noticeable wake interactions. Comparisons of the coupled results and CAMRAD II free wake analysis with flight test data are shown in Figure 12. Overall, the agreement between flight test and coupled results is respectable, although not as good as the previous cases. The phase, magnitude, and shape of the pitching moments curves are in particularly good agreement with the test data. The major discrepancies

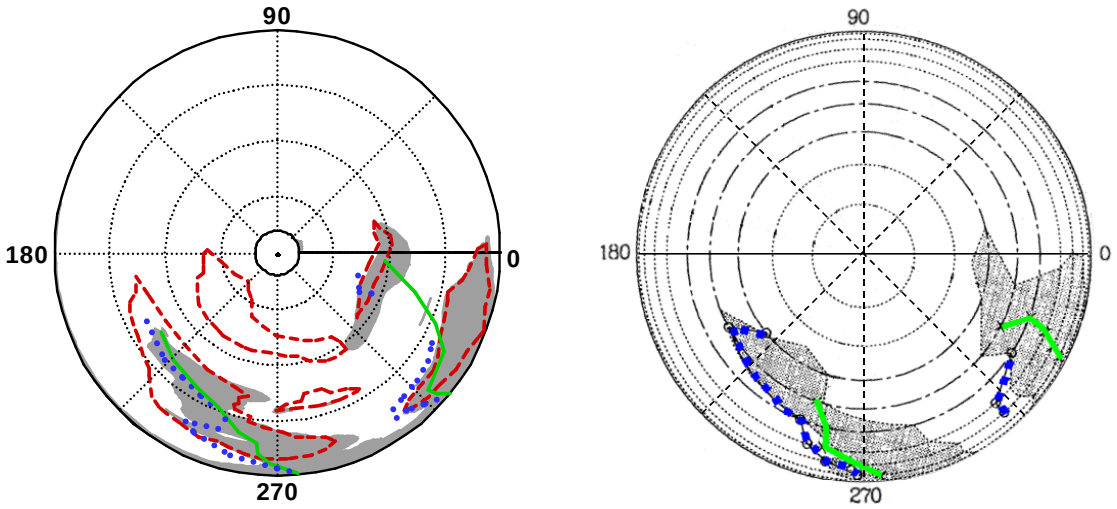

OVERFLOW/CAMRAD **FLIGHT TEST [38]**

Figure 13. Comparison of dynamic stall rotor maps, 0.24 advance ratio, high C_T
lift stall: ——, moment stall: ••••••, pressure coefficient divergence at x/c = 0.96: ▒▒▒, zero skin friction: – – –

between flight test and the coupled solution are in normal force prediction. On the advancing side there is considerable disagreement in the steepness with which the minimum peak loading region is entered and departed. The normal force distributions also lack the higher level and overshoot oscillations in the third quadrant. Based on wake visualization, this feature could be a blade-vortex interaction that is poorly captured.

Using various stall detection criteria, a dynamic stall rotor map is created in Figure 13 from flight test data [38, corrected] and CFD. Stall initiation lines based on normal force and pitching moment gradients are indicated. Regions of separation based on 96% chord upper surface pressure coefficient divergence from the mean are shaded. Regions of zero chordwise skin friction at 96% chord are also shown for the CFD solution. There is general agreement among all the stall/separation criteria. The dynamic stall regions between flight test and CFD are in remarkable agreement with initiation of both stall cycles at the correct locations. The only discrepancy is the inboard extent of the second cycle and the disconnect between the two CFD regions there. There is only mild stall inboard of r/R = 0.75, based on inconsistencies between the normal force, pitching moment, and pressure coefficient criteria in both analysis and flight test.

All the cases presented here were also investigated on a coarse grid obtained by taking every other point from the baseline grid. The normal force and pitching moment airloads were not sensitive to the grid density and were deemed grid converged. The only exception was the stall regions for the high thrust coefficient test point. The location of stall initiation and spanwise extent was somewhat sensitive to the grid details. This is not unexpected since CFD stall prediction can be highly grid and algorithm dependent. Two- and three-dimensional dynamic stall predictions are an area of ongoing research for which CFD has not yet been validated. Turbulence modeling remains one of the major challenges for accurate edge of the envelope and maneuver prediction for rotorcraft computations. However, for overall stall prediction, the coupled, turbulent, Navier-Stokes results are an improvement over table look-up with dynamic stall modeling in comprehensive codes.

In summary, the UH-60A coupled CFD/CSD aeroelastic calculations show a reasonable capability to accurately predict level flight airloads across a range of test conditions. CFD, in conjunction with corrections to flight test data, solved noted discrepancies in azimuthal phase lag and underprediction of pitching moments. Turbulence modeling and wake resolution and prediction issues continue to be the areas where further research is needed.

Quarter-Scale V-22 [35]

While normally referred to as a proprotor, the isolated V-22 rotor in cruise is an axial propeller. CFD computations can use the steady-state hover formulation when the angle of attack is zero. Calculations of the quarter-scale V-22 proprotor were performed by Romander [35] using a 1-bladed, one-third periodic domain grid system with 1.84 million points. Helical tip Mach numbers of approximately 0.64 and inflow ratios of 0.325 to 0.375 were simulated and compared with TRAM DNW experiments. Calculations underpredicted power by about 7% across a small range of thrust coefficients. In addition to the quarter-scale V-22, analyses were also performed on a NACA high-speed

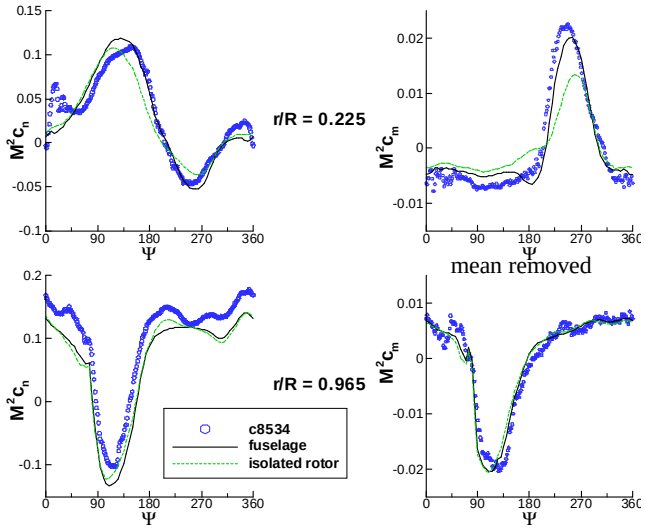

Figure 14. UH-60A rotor-fuselage interaction airloads comparison, 0.37 advance ratio.

propeller and full-scale V-22 rotor, which was compared against a Variable Diameter Tilt Rotor (VDTR).

Rotor-Fuselage Interaction

Addition of a fuselage to unsteady rotorcraft simulations creates the need to model bodies in relative motion. Overset grids are particularly suited for this difficult task. Numerous calculations have been performed for the V-22 in hover, low speed flight, and cruise [29,39,27] as well as the UH-60A in forward flight with a notional fuselage [26].

Full-Scale UH-60A [26]

The overset methodology and automatic background Cartesian meshes make adding a fuselage to an isolated rotor calculation a straightforward task. A low fidelity Blackhawk fuselage geometry (Figure 7) has been included in the high speed (c8534) coarse grid UH-60A calculation. CFD/CSD coupled airloads with and without the fuselage are compared with the flight test data in Figure 14. The primary effect of including the fuselage is to induce an upwash on the inboard part of the rotor blade ($r/R < 0.40$) near 180 degrees azimuth, thereby increasing the normal force in this region. The change on this part of the rotor affects the overall trim equilibrium and results in a slight redistribution of forces on the entire rotor disk. Of note is the significant improvement in pitching moment comparison in the reversed flow region ($r/R = 0.225$, $\Psi \approx 270$ deg) due to the presence of the fuselage. For this high speed flight condition the rotor-fuselage interactions are minimal.

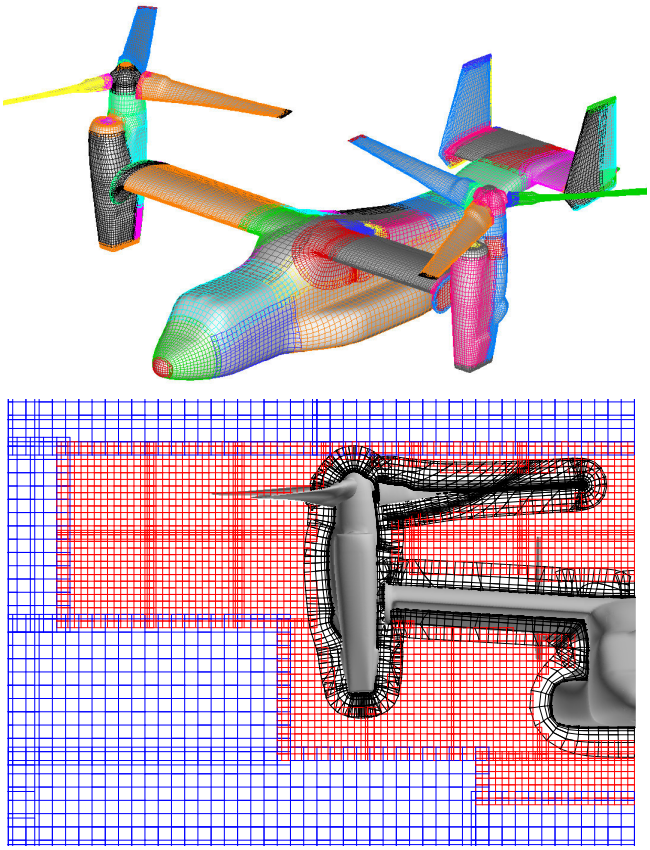

Figure 15. V-22 surface, near-, and off-body grid systems in hover.

Quarter-Scale V-22 [29,39,27]

Highlights will be shown here of rotor-fuselage V-22 simulations in hover and low speed flight conditions. A CFD model has been constructed of rotors installed on a high fidelity V-22 airframe hover configuration. The aircraft fuselage, wing with deflected flaps, nacelles in helicopter mode, and tail are modeled. Both full-span and half-span with image plane time-dependent CFD simulations were run. Rotor rotation on each wing is such that the blades pass from wing leading to trailing edge. The nacelle spinner rotates with the blades, sliding over a portion of the nacelle spinner collar. All near-body grids including the nacelles and fuselage are modeled as viscous. The level-1 off-body grids enclosed not only the rotor plane as in the isolated analysis but also the complete airframe, with the finest off-body grid spacing at 0.10 chords. Figure 15 shows the 109 overset surface grids and a streamwise cross-sectional cut through the half-span volume grid system. The total number of grid points in the full-span model is 47.6 million with 63% in the off-body grids. The half-span simulation has an inviscid plane of symmetry boundary condition at the centerline. Simulations were run for at least 30 rotor revolutions to remove initial transients. One rotor revolution

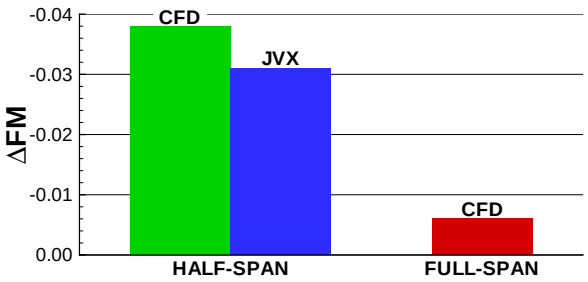

Figure 16. V-22 install half- and full-span vs. isolated rotor figure of merit increments.

uses 3200 iterations per revolution, corresponding to 0.1125 degrees per time step.

The first area under investigation is the difference between full- and half-span configurations in hover [29]. The rotor collective is 10 degrees and the hover tip Mach number is 0.625, corresponding to the quarter-scale V-22 test. Hover performance increments due to rotor installation when compared with isolated rotor calculations are summarized in Figure 16 for full- and half-span configurations. At the same C_T/σ, the JVX tiltrotor experimental data for a half-span wing model compared to the isolated rotor indicates good agreement [40]. The full-span CFD analysis shows a much smaller performance penalty.

An installation penalty occurs due to a fountain of recirculating flow that is formed by the presence of the wing and second rotor. Rotor performance is reduced as the blades pass over the wing and through the fountain. The differences in half- and full-span fountain flows can be seen in the CFD particle traces of Figure 17. The fountain is highly three-dimensional. The half-span calculation indicates a significantly larger fountain height and spanwise extent compared with the full-span calculation. Away from the fuselage, the organized wake of an isolated rotor is seen.

The half-span CFD calculation also shows increased airframe download/thrust (0.130) compared with the full-span calculation (0.100). The reduced full-span fountain flow results in lower download attributable to the fuselage and sponson components of the airframe. Figure 18 shows the time-averaged pressure force in the download direction for the full-span V-22 calculation. The details of the airframe download distribution are enlightening. Overall, the characteristics of the two fountain flows match the experimental flow visualizations by Polak [41] and download measurements agree with available test data. The CFD simulations suggest the importance of full-span tiltrotor wind tunnel testing.

A second area of investigation is the behavior of the V-22 tiltrotor hovering in low speed winds [39]. During V-22 critical azimuth flight testing designed to evaluate

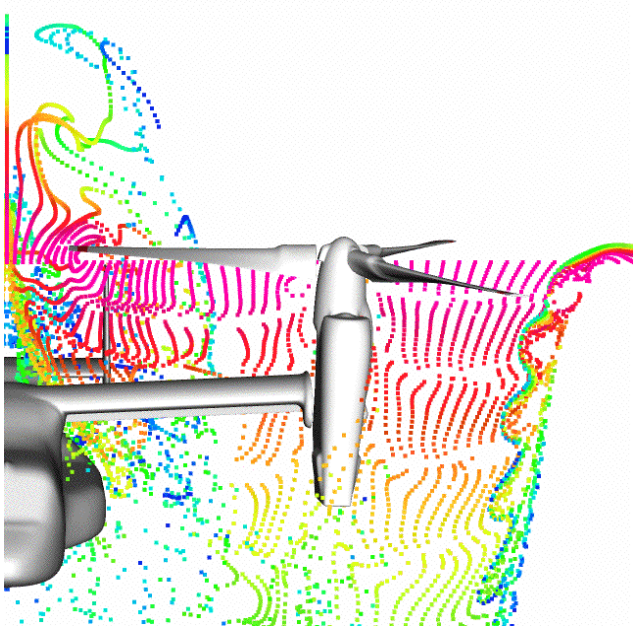

half-span

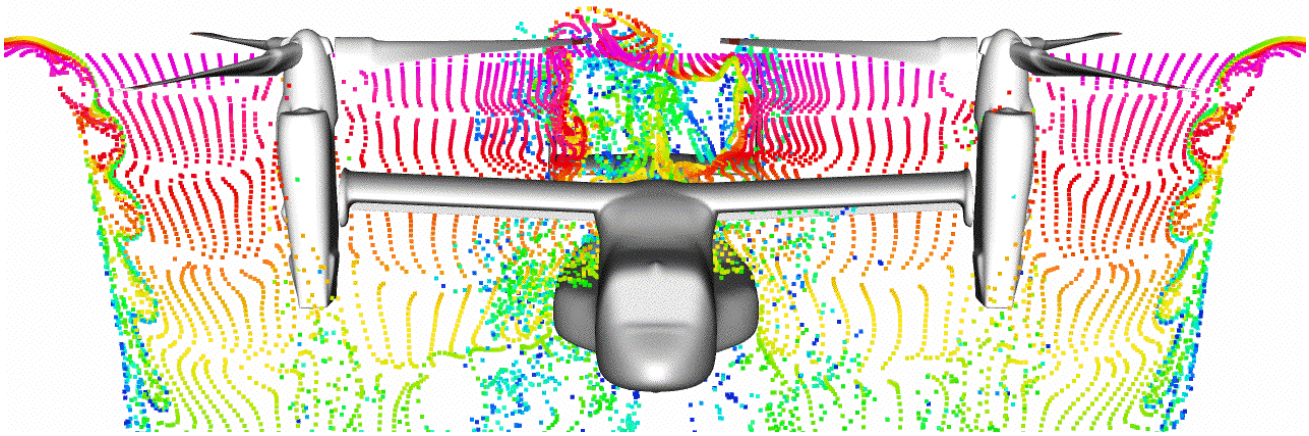

full-span

Figure 17. Time-dependent particle traces through V-22 simulations, colored by release time.

control margins and pilot workload, phenomena such as pitch-up with sideslip (PUWSS) and increased power required in sideward flight were identified [41]. Critical azimuth CFD solutions were run at a fixed 14-degrees collective ($C_T \approx 0.015$), zero fuselage pitch angle, and no trim considerations. Simulations were run for 0, 45, 90, 135, and 180 degrees wind azimuth at a 35-knot wind speed. A hover tip Mach number of 0.736 corresponds to the full-scale V-22. To determine rotor-fuselage interference effects, steady simulations with the rotors not turning were also computed.

PUWSS is a well-understood aeromechanics phenomenon in which the upwind rotor wake impinges on the horizontal tail causing the aircraft to pitch up. The phenomenon is most critical with wind from ±45° azimuths, although it occurs in a range from 30 to 70 degrees. In the CFD calculations, PUWSS is noted as an increase in airframe pitching moment, which is equilibrated to a tip path plane tilt (longitudinal flapping) required to counteract the moment. Positive tip path plane tilt (flap down in front) counteracts a nose up pitching moment. Time-averaged values of download/thrust and tip path plane tilt are shown in Figure 19 for a 35-knot wind speed as a function of wind direction, with and without rotors. Note that the pitch-up is not indicated in the rotors-off calculations, confirming that this is an adverse rotor-airframe interaction. Calculated pitch-up trends are in excellent agreement with flight test observations [42].

In V-22 critical azimuth testing the power required to hover in sidewinds is 10-20% higher than no/low-wind hover. In constant high wind conditions, the power required to hover increases drastically (up to 80%) as the wind direction moves from a headwind towards a sidewind. CFD clearly shows this to be an adverse rotor-fuselage interaction due to an increase in airframe download (Figure 19). Airframe download visualizations similar to Figure 18 pinpoint the wing upper surface, fuselage underside, and cargo ramp as significant sources of download. Developing an experimental model that can be turned through 180° of sideslip without interfering with the fuselage flowfield is difficult. Calculations, however, have shown this to be a tractable problem for CFD.

V-22 calculations in airplane mode with individual blades have been limited. It has often been assumed that individual blade modeling is not necessary for cruise conditions and that the integrated effects of an actuator disk are sufficient. Meakin [27] calculated the full-scale V-22 in high speed forward flight (Mach 0.445) on a grid with 27.8 million points: 8 million near-body and 19.8 million off-body. The large number of off-body grid points are required to capture the wake as it convects completely past the fuselage. A flow visualization is shown in Figure 20. Particles are emitted from the blade tips and are convected downstream with minimal wake-fuselage interaction.

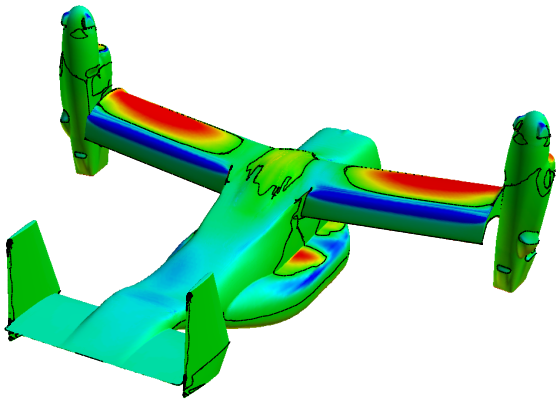

Figure 18. V-22 time-averaged airframe download pressure component in hover: red – download, blue – upload, black line – zero contour.

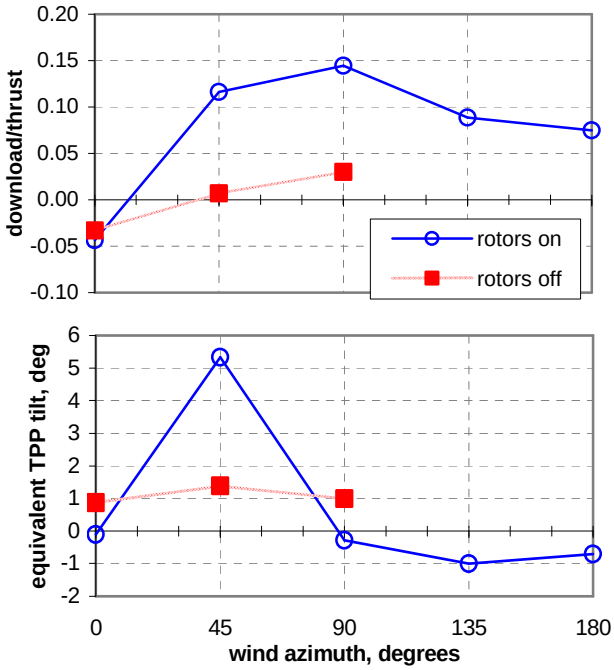

Figure 19. V-22 time-averaged airframe download and equivalent TPP tilt, 35-knot wind.

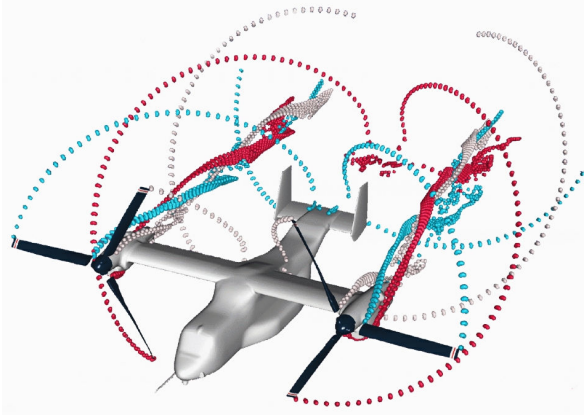

Figure 20. V-22 in cruise, Mach 0.445.

CONCLUDING REMARKS

Computational fluid dynamics for rotorcraft applications has made considerable progress in recent years. One of the enabling technologies has been the use of overset grid methodologies for dynamic, time-dependent, moving body, viscous flow simulations. Rotorcraft configurations are characterized by complex geometry and flow features. Overset grid software is shown to naturally handle the geometric complexity and bodies in relative motion. Parallel processing is readily implemented to take advantage of high performance computing. Application to the UH-60A Blackhawk helicopter and V-22 Osprey tiltrotor have been demonstrated for hover, forward flight, and rotor-fuselage interaction configurations. CFD favorably predicts hover performance, rotor airloads for a range of flight conditions, and rotor-fuselage interaction aeromechanics phenomenon. Aeroelastic effects are considered by coupling with a rotorcraft comprehensive code. Wake resolution and turbulence modeling remain challenges for accurate prediction of the entire flow field across the complete flight regime.

ACKNOWLEDGEMENTS

The computer resources of the Department of Defense Major Shared Resource Centers (MSRC) and the NASA Advanced Supercomputing (NAS) Division are gratefully acknowledged.

REFERENCES

1. Duraisamy, K., Baeder, J., and Sitaraman, J., "High Resolution Wake Capturing Methodology for Improved Rotor Aerodynamic Computations," American Helicopter Society 61st Annual Forum, Grapevine, TX, June 2005.

2. Renaud, T., O'Brien, D., Smith, M., and Potsdam, M., "Evaluation of Isolated Fuselage and Rotor-Fuselage Interaction Using CFD," American Helicopter Society 60th Annual Forum, Baltimore, MD, June 2004.

3. Ruffin, S., O'Brien, D., Smith, M., Hariharan, N., Lee, J., and Sankar, L., "Comparison of Rotor-Airframe Interaction Utilizing Overset and Unstructured Grid Techniques," AIAA 2004-0046, 42nd AIAA Aerospace Sciences Meeting and Exhibit, Reno, NV, January 2004.

4. Bauchau, O. A., and Ahmad, J. U., "Advanced CFD and CSD Methods for Multidisciplinary Applications in Rotorcraft Problems," AIAA 1996-4151, AIAA/ NASA/ISSMO 6th Symposium on Multidisciplinary Analysis and Optimization, Reston, VA, September 1996.

5. Costes, M., Pahlke, K., D'Alascio, A., Castellin, C., and Altmikus, A., "Overview of Results Obtained During the 6-Year French-German CHANCE Project," American Helicopter Society 61st Annual Forum, Grapevine, TX, June 2005.

6. Renaud, T., "Unsteady Euler and Navier-Stokes Computations of a Complete Helicopter," 31st European Rotorcraft Forum, Florence, Italy, September 2005.

7. Benoit, C., and Jeanfaivre, G., "Three-Dimensional Inviscid Isolated Rotor Calculations Using Chimera and Automatic Cartesian Partitioning Methods," *Journal of the American Helicopter Society*, Vol. 48, No. 2, April 2005, pp. 128-138.

8. Pomin, H. and Wagner, S., "Navier-Stokes Analysis of Helicopter Rotor Aerodynamics in Hover and Forward Flight," AIAA 2001-0998, 39th Aerospace Sciences Meeting and Exhibit, Reno, NV, January 2001.

9. Park, Y., Nam, H., and Kwon, O., "Simulation of Unsteady Rotor-Fuselage Interactions Using Unstructured Adaptive Meshes," American Helicopter Society 59th Annual Forum, Phoenix, AZ, May 2003.

10. Steger, J., Dougherty, F. C., and Benek, J., "A Chimera Grid Scheme," Advances in Grid Generation, K. N. Ghia and U. Ghia, eds., ASME FED Vol. 5, June 1983.

11. Noack, R. W., "DiRTlib: A Library to Add an Overset Capability to Your Flow Solver," AIAA 2005-2116, 17th AIAA Computational Fluid Dynamics Conference, Toronto, Canada, June 2005.

12. Noack, R. W., "SUGGAR: A General Capability for Moving Body Overset Grid Assembly," AIAA 2005-2117, 17th AIAA Computational Fluid Dynamics Conference, Toronto, Canada, June 2005.

13. Chan, W. M., "The OVERGRID Interface for Computational Simulations on Overset Grids," AIAA 2002-3188, 32nd AIAA Fluid Dynamics Conference, St. Louis, MO, June 2002.

14. Chan, W. M., Gomez, R. J., Rogers, S. E., and Buning, P. G., "Best Practices in Overset Grid Generation," AIAA 2002-3191, 32nd AIAA Fluid Dynamics Conference, St. Louis, MO, June 2002.

15. Meakin, R. L., "Automatic Off-Body Grid Generation for Domains of Arbitrary Size," AIAA 2001-2536, 15th AIAA Computational Fluid Dynamics Conference, Anaheim, CA, June 2001.

16. Chan, W. M., and Buning, P. G., "User's Manual for FOMOCO Utilities – Force and Moment Computation Tools for Overset Grids," NASA Technical Memorandum 110408, July 1996.

17. Chan, W. M., and Buning, P. G., "Zipper Grids for Force and Moment Computation on Overset Grids," AIAA 1995-1681, 12th AIAA Computational Fluid Dynamics Conference, San Diego, CA, June 1995.

18. Buning, P. G., Gomez, R. J., and Scallion, W. I., "CFD Approaches for Simulation of Wing-Body Stage Separation," 22nd AIAA Applied Aerodynamics Conference, Providence, RI, August 2004.

19. Chan, W. M., Meakin, R. L., and Potsdam, M. A., "CHSSI Software for Geometrically Complex Unsteady Aerodynamic Applications," AIAA 2001-0593, 39th Aerospace Sciences Meeting and Exhibit, Reno, NV, January 2001.

20. Buning, P. G., et al., "OVERFLOW User's Manual, Version 1.8ab," NASA Langley Research Center, July 2003.

21. Jespersen, D. J., Pulliam, T. H., and Buning, P. G., "Recent Enhancements to OVERFLOW," AIAA 1997-0644, 35th Aerospace Sciences Meeting and Exhibit, Reno, NV, January 1997.

22. Strawn, R. C. and Djomehri, M. J., "Computational Modeling of Hovering Rotor and Wake Aerodynamics," *Journal of Aircraft*, Vol. 39, No. 5, 2002, pp. 786-793.

23. Nygaard, T. A., Dimanlig, A. C., and Meadowcroft, E. T., "Application of a Momentum Source Model to the RAH-66 Comanche FANTAIL," American Helicopter Society 4th Decennial Specialist's Conference on Aeromechanics, San Francisco, CA, January 2004.

24. Murman, S., Chan, W., Aftosmis, M., and Meakin, R., "An Interface for Specifying Rigid-Body Motions for CFD Applications," AIAA 2003-1237, 41st Aerospace Sciences Meeting and Exhibit, Reno, NV, January 2003.

25. Meakin, R. L., "Object X-Rays for Cutting Holes in Composite Overset Structured Grids," AIAA 2001-2537, 15th AIAA Computational Fluid Dynamics Conference, Anaheim, CA, June 2001.

26. Potsdam, M., Yeo, H., and Johnson, W., "Rotor Airloads Prediction Using Loose Aerodynamic/ Structural Coupling," American Helicopter Society 60th Annual Forum, Baltimore, MD, June 2004.

27. Meakin, R. L. and Wissink, A. M., "Unsteady Aerodynamic Simulation of Static and Moving Bodies Using Scalable Computers," AIAA 1999-3302, 14th AIAA Computational Fluid Dynamics Conference, Norfolk, VA, July 1999.

28. Buning, P. G., and Cable, S. B., "Benchmarking OVERFLOW 2, a Structured CFD Code," ERDC Major Shared Resource Center Resource, Spring 2005, http://www.erdc.hpc.mil/pubs/pdf/spring05.pdf, pp. 16-17.

29. Potsdam, M. A. and Strawn, R. C., "CFD Simulations of Tiltrotor Configurations in Hover," *Journal of the American Helicopter Society*, Vol. 50, No. 1, January 2005, pp. 82-94.

30. Ruzicka, G., Strawn, R., and Meadowcroft, E., "Discrete CFD Analysis of Ducted Tail Fan Flow," AIAA 2004-0048, 42nd AIAA Aerospace Sciences Meeting and Exhibit, Reno, NV, January 2004.

31. Kunz, P., and Strawn, R., "Analysis and Design of Rotors at Ultra-Low Reynolds Numbers," AIAA 2002-0099, 40th AIAA Aerospace Sciences Meeting and Exhibit, Reno, NV, January 2002.

32. Korfeld, K., Strawn, R., and Long, L., "Computational Analysis of a Prototype Martian Rotorcraft Experiment," AIAA 2002-2815, 20th AIAA Applied Aerodynamics Conference, St. Louis, MO, June 2002.

33. Lorber, P. F., Stauter, R. C., and Landgrebe, A. J., "A Comprehensive Hover Test of the Airloads and Airflow of an Extensively Instrumented Model Helicopter Rotor," American Helicopter Society 45th Annual Forum, Boston, MA, May 1989.

34. Johnson, W., "Calculation of Tilt Rotor Aeroacoustic Model (TRAM DNW) Performance, Airloads, and Structural Loads," American Helicopter Society Aeromechanics Specialists' Meeting, Atlanta, GA, November 2000.

35. Romander, E., "Computational Simulation of Propellers in Cruise," 23rd International Congress of Aeronautical Sciences (ICAS), Toronto, Canada, September 2002.

36. Kufeld, R. M., Balough, D. L., Cross, J. L., Studebaker, K. F., Jennison, C. D., and Bousman, W. G., "Flight Testing of the UH-60A Airloads Aircraft," American Helicopter Society 50th Annual Forum, Washington, D.C., May 1994.

37. Kufeld, R. M., and Bousman, W. G., "UH-60A Airloads Program Azimuth Reference Correction," *Journal of the American Helicopter Society*, Vol. 50, No. 2, April 2005, pp. 211-213.

38. Bousman, W. G., "A Qualitative Examination of Dynamic Stall from Flight Test Data," American Helicopter Society 53rd Annual Forum, Virginia Beach, VA, April 1997.

39. Potsdam, M. A., Schaller, D. F., Rajagopalan, R. G., and Silva, M. J., "Tiltrotor Aeromechanics Phenomena in Low Speed Flight," American Helicopter Society 4th Decennial Specialist's Conference on Aeromechanics, San Francisco, CA, January 2004.

40. Felker, F. F., Signor, D. B., Young, L. A., and Betzina, M. D., "Performance and Loads Data from a Hover Test of a 0.658-Scale V-22 Rotor and Wing," NASA TM 89419, April 1987.

41. Polak, D. R., Rehm, W., and George, A. R., "Effects of an Image Plane on the Tiltrotor Fountain Flow," *Journal of the American Helicopter Society*, April 2000, pp. 90-96.

42. Klein, G., Roberts, B., and Seymour, C., "MV-22 Handling Qualities Flight Test Summary," American Helicopter Society 56th Annual Forum, Virginia Beach, VA, May 2000.